# Multi-electron excitation contributions towards the primary and satellite states in the photoelectron spectrum. Supplementary Information

Torsha Moitra, Alexander C. Paul, Piero Decleva, Henrik Koch, and Sonia Coriani
email: henrik.koch@sns.it, soco@kemi.dtu.dk

## Scaling of the CC3 contributions

Table S1: Asymptotic scaling of the most important steps in the calculation of CC3 Dyson orbitals in floating point operations (FLOP) in terms of the number of occupied ($n_\mathrm{o}$) and virtual ($n_\mathrm{v}$) orbitals.

| Parameters | Scaling [FLOP] |
|---|---|
| $t_\mu$ | $4n_\mathrm{v}^4 n_\mathrm{o}^3$ |
| $\lambda_\mu$ | $8n_\mathrm{v}^4 n_\mathrm{o}^3$ |
| $L_\mu$ | $8n_\mathrm{v}^4 n_\mathrm{o}^3$ |
| $R_\mu$ | $8n_\mathrm{v}^4 n_\mathrm{o}^3$ |
| $\gamma_p^L$ | $6n_\mathrm{v}^4 n_\mathrm{o}^3$ |
| $\gamma_p^R$ | $8n_\mathrm{v}^4 n_\mathrm{o}^3$ |

## Parameters used in the LCAO B-spline TD-DFT calculations

Table S2: Parameters used in the LCAO B-spline code. $L_\mathrm{max}$ and $l_\mathrm{max}$ are the maximum angular momentum employed in the one center expansion at the origin and on each off-center atom, respectively. $R_\mathrm{max}$ and $r_\mathrm{max}$ (both in a.u.) are the maximum radial grid length from origin and from the off-center atoms, respectively. $n_\mathrm{step}$ is the number of radial grid points used.

| Molecule | $n_\mathrm{step}$ | $L_\mathrm{max}$ | $R_\mathrm{max}$ | LCAO descriptor | |
|---|---|---|---|---|---|
| | | | | $l_\mathrm{max}$ | $r_\mathrm{max}$ |
| $H_2O$ | 100 | 10 | 25.0 | 2(O) | 1.000(H) |
| CS | 100 | 12 | 25.0 | 2(C,S) | 0.400 (S), 0.600(C) |
| $H_2S$ | 100 | 12 | 25.0 | 1(H) | 0.600(H) |
| $CS_2$ | 100 | 20 | 25.0 | 2(S) | 1.000(S) |
| $C_3H_6O$ | 100 | 12 | 25.0 | 2(C,O), 1(H) | 0.600(O), 1.000(C,H) |

# Ground state electronic configuration

Table S3: Hartree-Fock ground-state electronic configurations.

| Molecule | Configuration |
|---|---|
| $H_2O$ | $1a_1^2 2a_1^2 1b_2^2 3a_1^2 1b_1^2$ |
| CS | $1\sigma^2 2\sigma^2 3\sigma^2 4\sigma^2 1\pi^4 5\sigma^2 6\sigma^2 7\sigma^2 2\pi^4$ |
| $H_2S$ | $1a_1^2 2a_1^2 1b_2^2 3a_1^2 1b_1^2 4a_1^2 2b_2^2 5a_1^2 2b_1^2$ |
| $CS_2$ | $1\sigma_u^2 1\sigma_g^2 2\sigma_g^2 2\sigma_u^2 3\sigma_g^2 3\sigma_u^2 4\sigma_g^2 1\pi_g^4 1\pi_u^4 5\sigma_g^2 4\sigma_u^2 6\sigma_g^2 5\sigma_u^2 2\pi_u^4 2\pi_g^4$ |

# Largest amplitudes and weight of single excitations for given ionizations

Table S4: CS: Dominant amplitudes and amount of single excitation contributions to the ionization bands. The ionization energies and intensities are reported in Table 2. Only configurations having amplitudes $R_i^{\mathfrak{b}}$ and $R_{ij}^{\mathfrak{b}b}$ greater than 0.3 and 0.4 for singles and doubles excitations, respectively, are listed.

| Peak | EOM-CCSD | | | EOM-CC3 | | |
|---|---|---|---|---|---|---|
| | Dominant config. | $\mid R_1/R \mid$ | $\mid L_1/L \mid$ | Dominant config. | $\mid R_1/R \mid$ | $\mid L_1/L \mid$ |
| X $^2\Sigma$ | $7\sigma^{-1}$ | 0.96 | 0.89 | $7\sigma^{-1}$ | 0.94 | 0.87 |
| A $^2\Pi$ | $2\pi^{-1}$ | 0.98 | 0.95 | $2\pi^{-1}$ | 0.97 | 0.94 |
| B $^2\Sigma$ | $6\sigma^{-1}$ | 0.90 | 0.85 | $6\sigma^{-1}$,$2\pi^{-1}(7\sigma^{-1}3\pi)$ | 0.67 | 0.63 |
| C $^2\Sigma$ | $6\sigma^{-1}$, $2\pi^{-1}(7\sigma^{-1}3\pi)$ | 0.37 | 0.26 | $6\sigma^{-1}$,$2\pi^{-1}(7\sigma^{-1}3\pi)$ | 0.73 | 0.53 |

Table S5: $H_2S$: Dominant amplitudes and amount of single excitation contribution to the ionization bands obtained at EOM-CC3/aug-cc-pVTZ level, as reported in Table 3. Ionization energies are in eV. Only configurations having amplitudes $R_i^{\mathfrak{b}}$ and $R_{ij}^{\mathfrak{b}b}$ greater than 0.3 and 0.4 for singles and doubles excitations, respectively, are listed.

| Peak | IE | Dominant config. | $\mid R_1/R \mid$ | $\mid L_1/L \mid$ |
|---|---|---|---|---|
| X $^2B_1$ | 10.38 | $2b_1^{-1}$ | 0.98 | 0.95 |
| A $^2A_1$ | 13.40 | $5a_1^{-1}$ | 0.97 | 0.93 |
| B $^2B_2$ | 15.64 | $2b_2^{-1}$ | 0.97 | 0.93 |
| | 19.35 | $2b_1^{-2}5b_2$, $2b_1^{-2}4b_2$ | 0.07 | 0.07 |
| | 20.29 | $4a_1^{-1}$, $2b_1^{-2}9a_1$, $2b_1^{-2}8a_1$, $2b_1^{-2}6a_1$ | 0.28 | 0.27 |
| | 22.27 | $4a_1^{-1}$, $2b_1^{-2}6a_1$ | 0.50 | 0.49 |
| | 22.62 | $2b_1^{-1}(5a_1^{-1}8a_1)$, $2b_1^{-1}(5a_1^{-1}6a_1)$, $2a_1^{-1}(5a_1^{-1}9a_1)$ | 0.02 | 0.16 |
| | 23.26 | $4a_1^{-1}$, $2b_1^{-2}10a_1$ | 0.34 | 0.33 |
| | 23.72 | $4a_1^{-1}$, $2b_1^{-2}10a_1$ | 0.41 | 0.39 |

Table S6: $CS_2$: Dominant amplitudes and amount of single excitation contribution towards ionization bands obtained at EOM-CCSD/aug-cc-pVDZ level of theory, as reported in Table 4. Ionization energies are in eV. Only configurations having amplitudes $R_i^{\mathfrak{b}}$ and $R_{ij}^{\mathfrak{b}b}$ greater than 0.3 and 0.4 for singles and doubles excitations, respectively, are listed.

| Peak | IE | Dominant config. | $\mid R_1/R \mid$ | $\mid L_1/L \mid$ |
|---|---|---|---|---|
| X $^2\Pi_g$ | 9.90 | $2\pi_g^{-1}$ | 0.98 | 0.93 |
| A $^2\Pi_u$ | 13.20 | $2\pi_u^{-1}$ | 0.93 | 0.87 |
| B $^2\Sigma_u$ | 14.45 | $5\sigma_u^{-1}$ | 0.96 | 0.89 |
| $^2\Pi_u$ | 17.78 | $2\pi_g^{-2}3\pi_u$ | 0.14 | 0.09 |
| C $^2\Sigma_g$ | 16.42 | $6\sigma_g^{-1}$ | 0.93 | 0.85 |
| D $^2\Pi_u$ | 21.68 | $2\pi_u^{-1}$, $2\pi_g^{-2}3\pi_u$ | 0.32 | 0.16 |

Table S7: $CS_2$: Dominant amplitudes and amount of single excitation contribution towards ionization bands obtained at EOM-CC3/aug-cc-pVDZ level of theory, as reported in Table 4. Ionization energies are in eV. Only configurations having amplitudes $R_i^{\mathfrak{b}}$ and $R_{ij}^{\mathfrak{b}b}$ greater than 0.3 and 0.4 for singles and doubles excitation, respectively, are listed.

| Peak | IE | Dominant config. | $\mid R_1/R \mid$ | $\mid L_1/L \mid$ |
|---|---|---|---|---|
| X $^2\Pi_g$ | 9.84 | $2\pi_g^{-1}$ | 0.97 | 0.91 |
| A $^2\Pi_u$ | 12.74 | $2\pi_u^{-1}$, $2\pi_g^{-2}3\pi_u$ | 0.86 | 0.83 |
| B $^2\Sigma_u$ | 14.20 | $5\sigma_u^{-1}$ | 0.94 | 0.87 |
| $^2\Pi_u$ | 14.74 | $2\pi_g^{-2}3\pi_u$ | 0.23 | 0.13 |
| $^2\Pi_u$ | 15.82 | $2\pi_g^{-2}3\pi_u$ | 0.08 | 0.08 |
| C $^2\Sigma_g$ | 15.93 | $6\sigma_g^{-1}$ | 0.86 | 0.81 |
| D $^2\Pi_u$ | 17.60 | $2\pi_u^{-1}$, $2\pi_g^{-2}3\pi_u$ | 0.43 | 0.31 |

## $H_2O$

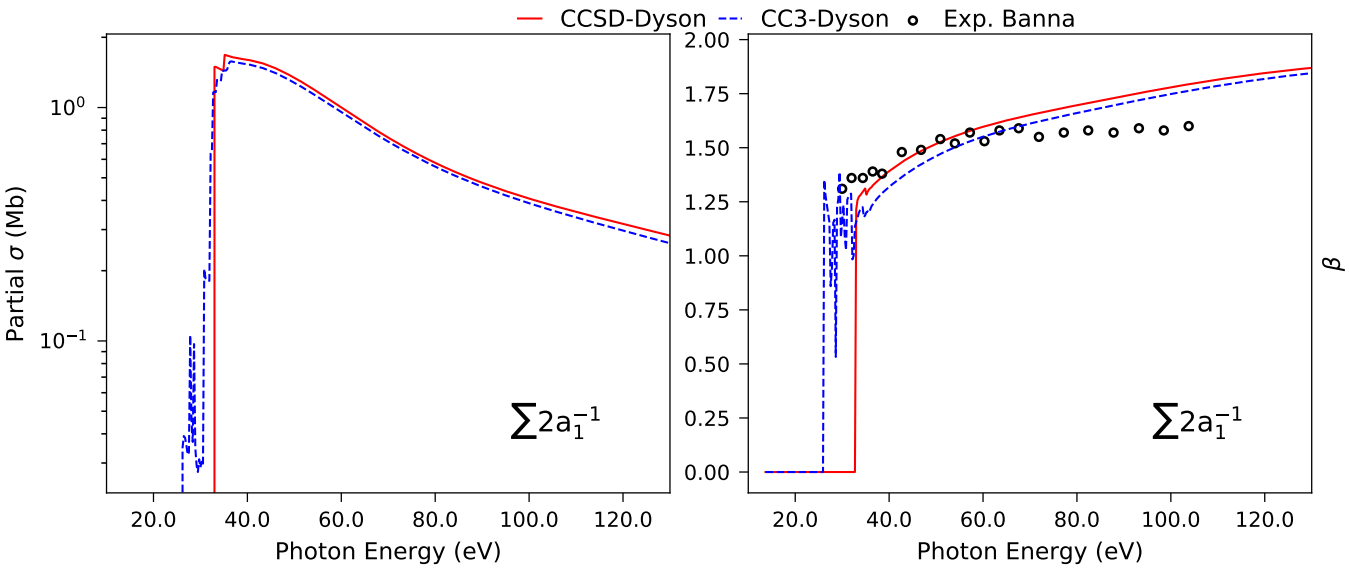


Figure S1: $H_2O$. (Combined) partial cross-section and (average) asymmetry parameter for the inner-valence $2a_1$ ionization channel, lumping together the two $2a_1^{-1}$ states at the CCSD level, and all CC3 states that contain a $2a_1^{-1}$ amplitude. Experimental results are taken from Ref. [1].

## CS

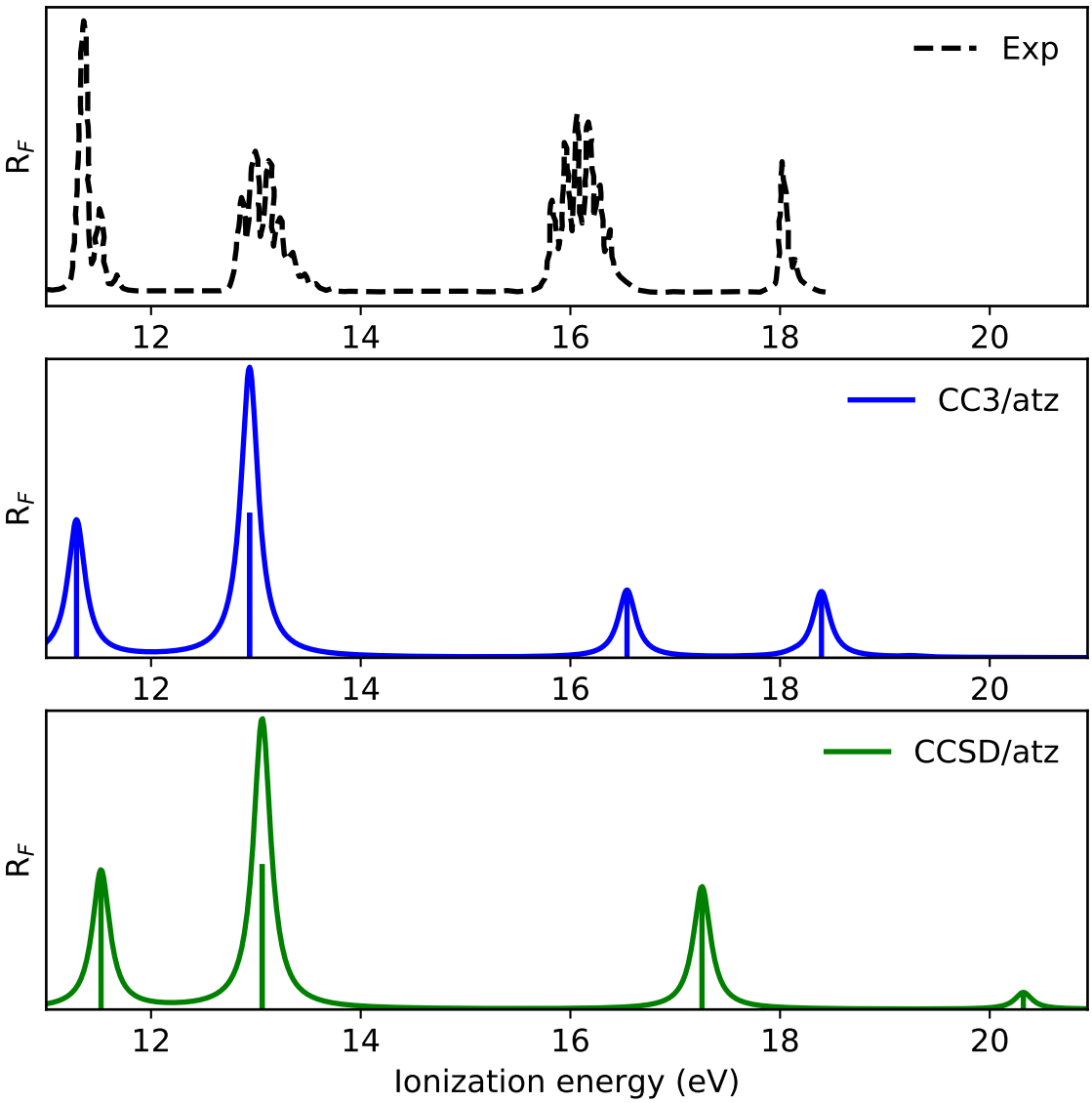


Figure S2: CS: Photoelelectron spectrum obtained using EOM-CCSD and EOM-CC3, aug-cc-pVTZ basis set. Experimental PES taken from Ref. [2]. Due to the use of pole strengths as measure of the intensity, the relative intensities are not accurately reproduced.[3]

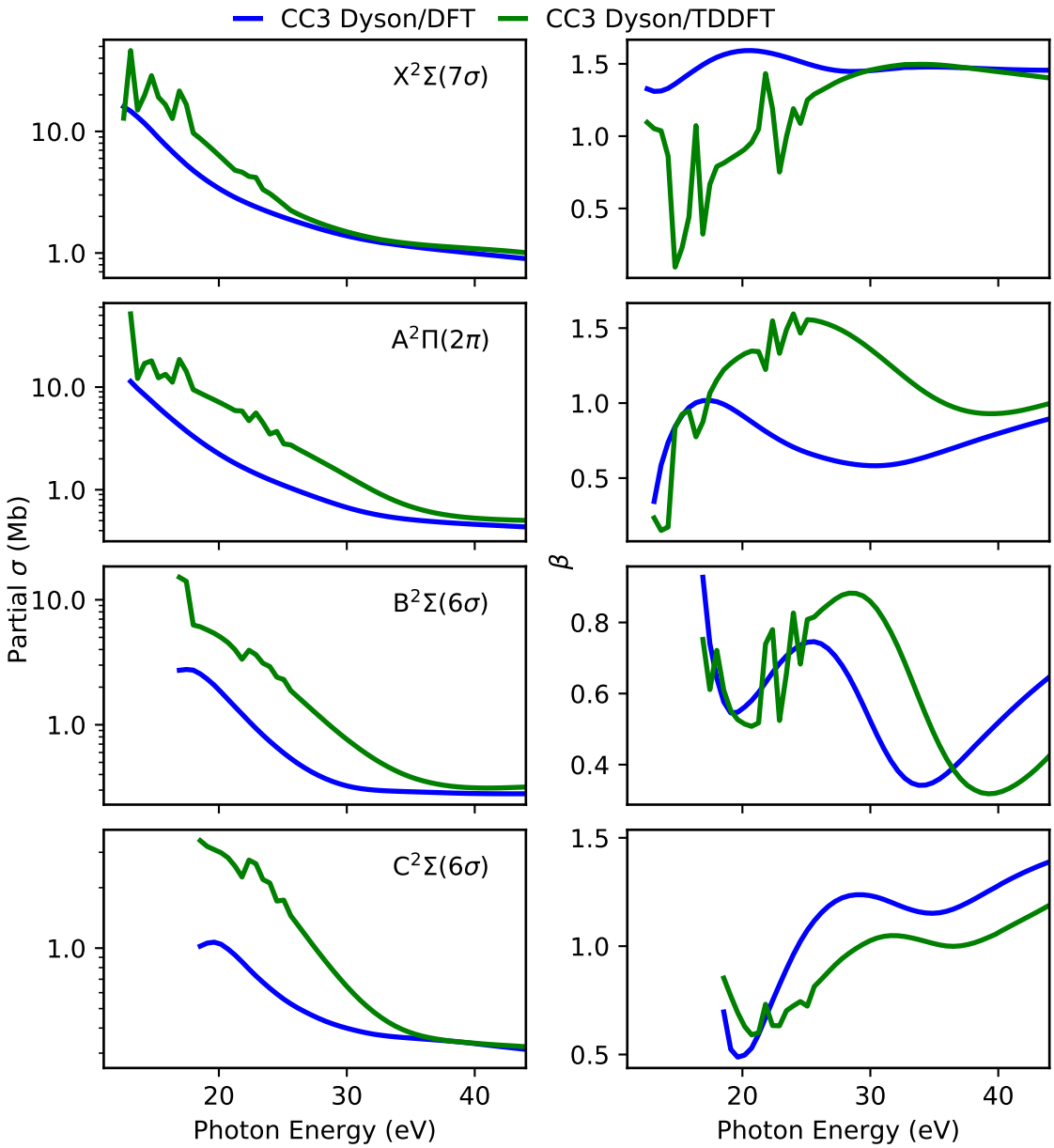


Figure S3: CS: Partial cross section and asymmetry parameters computed using EOM-CC3/aug-cc-pVTZ Dyson.

## $H_2S$

Table S8: $H_2S$: Comparison of ionization energies (eV) between Koopmans' theorem based Hartree-Fock molecular orbital, EOM-CCSD and EOM-CC3. Experimental ionization energies are from Ref. [4].

| Band | Ioniz. | Major MO | HF/aVTZ | EOM-CCSD/aVTZ IE | EOM-CCSD/aVTZ $R_F$ | EOM-CC3/aVTZ IE | EOM-CC3/aVTZ $R_F$ | EOM-CC3/aVDZ IE | EOM-CC3/aVDZ $R_F$ | Exp |
|---|---|---|---|---|---|---|---|---|---|---|
| X | $B_1$ | $2b_1$ | 10.48 | 10.42 | 0.9209 | 10.38 | 0.9051 | 10.18 | 0.9112 | 10.5 |
| A | $A_1$ | $5a_1$ | 13.66 | 13.43 | 0.9128 | 13.40 | 0.8935 | 13.26 | 0.8981 | 13.4 |
| B | $B_2$ | $2b_2$ | 16.05 | 15.69 | 0.9141 | 15.64 | 0.8927 | 15.57 | 0.8983 | 15.6 |
| | $B_2$ | $2b_2$ | | 21.98 | 0.0019 | 19.35 | 0.0047 | 19.32 | 0.0041 | 18* |
| | $A_1$ | $4a_1$ | | 22.41 | 0.4130 | 20.29 | 0.0709 | 20.10 | 0.0570 | 20 (19.6) |
| | $A_1$ | $4a_1$ | 26.75 | 24.35 | 0.2617 | 22.27 | 0.2268 | 22.17 | 0.2647 | 22.1 |
| | $B_1$ | $2b_1$ | | | | 22.62 | 0.0007 | 22.39 | 0.0009 | 22.7 |
| | $B_1$ | $2b_1$ | | | | | | 23.34 | 0.0010 | |
| Sat | $A_1$ | $4a_1$ | | 26.26 | 0.0232 | 23.26 | 0.1026 | 23.48 | 0.1654 | 23.05 |
| | $A_1$ | $4a_1$ | | | | 23.72 | 0.1576 | 23.87 | 0.0636 | 23.31 |
| | $A_1$ | $4a_1$ | | | | | | 24.39 | 0.0111 | |
| | $B_1$ | $2b_1$ | | | | | | 24.39 | 0.0077 | |

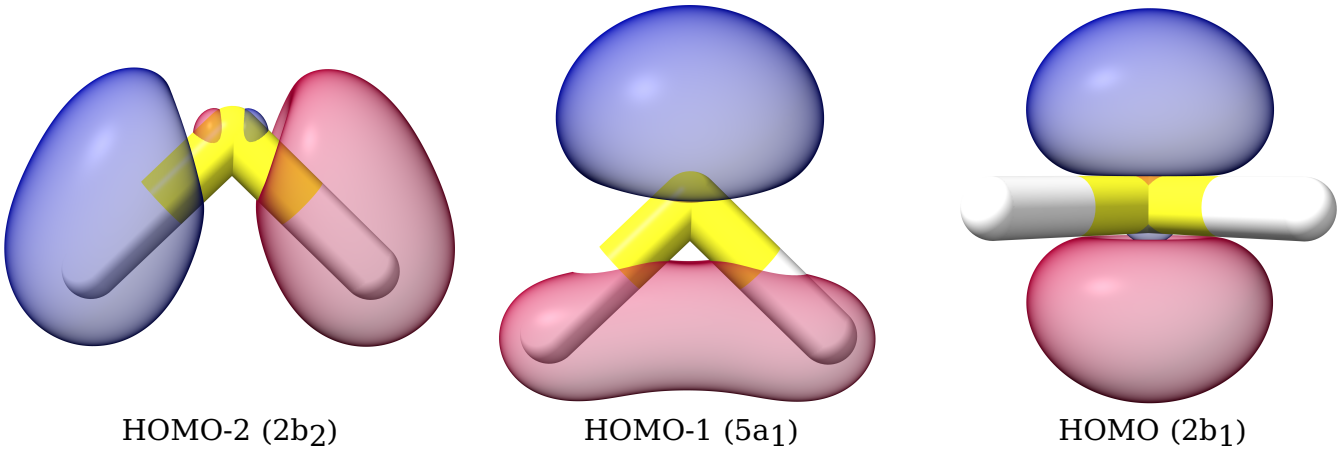


Figure S4: $H_2S$: Highest occupied molecular orbitals plotted at isovalues of 0.1. The orbital energies are −16.05 eV, −13.66 eV and −10.49 eV, respectively.

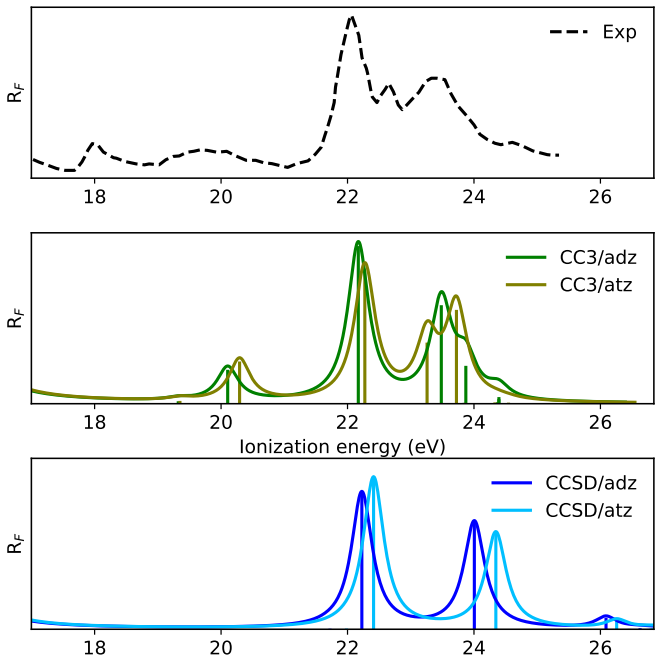


Figure S5: $H_2S$: Photoelelectron spectrum above 17 eV, obtained using EOM-CCSD and EOM-CC3, aug-cc-pVTZ basis set. Experimental PES taken from Ref. [4], with $h\nu = 90$ eV. The peak at 18 eV in experiment is attributed to OCS impurity.

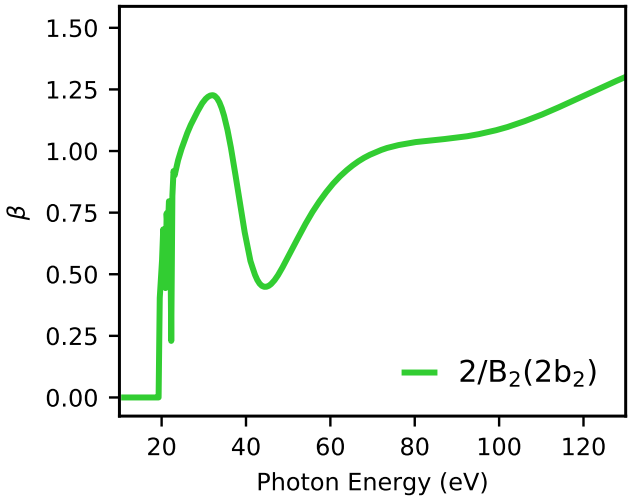


(a) IE = 19.35 eV

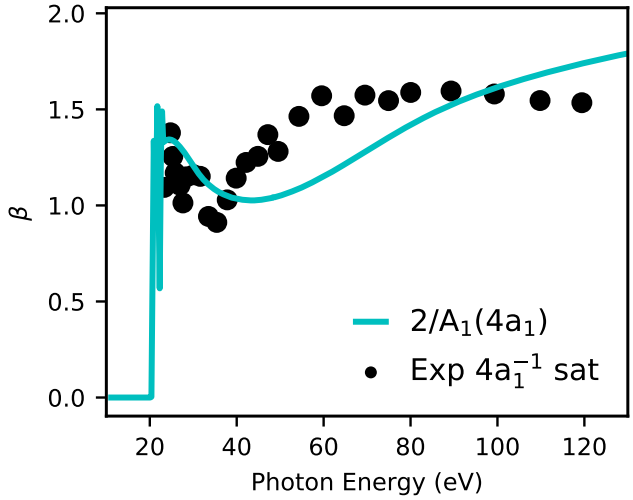


(b) IE = 20.29 eV

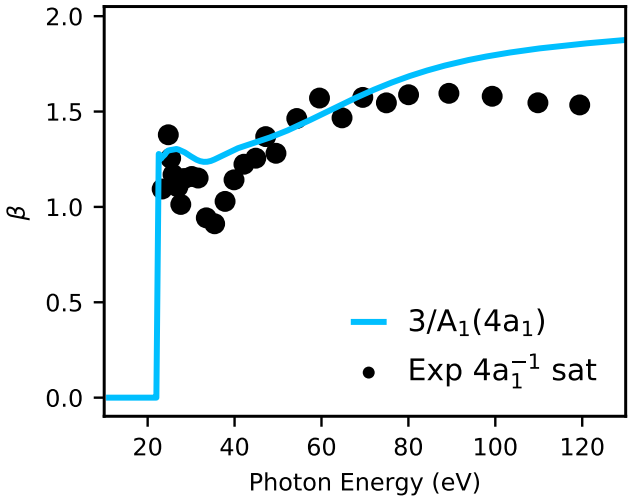


(c) IE = 22.27 eV

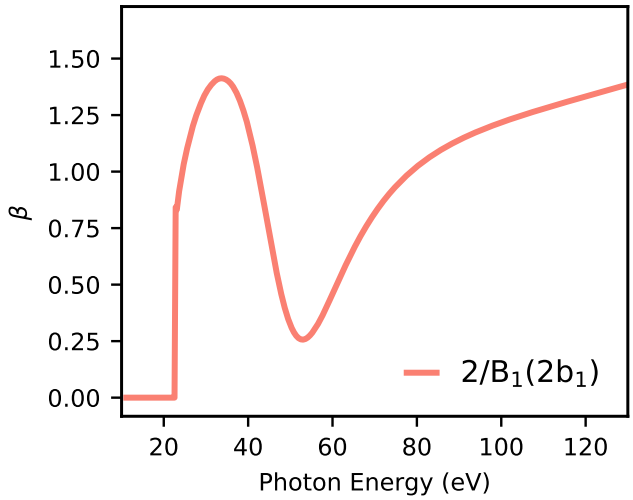


(d) IE = 22.62 eV

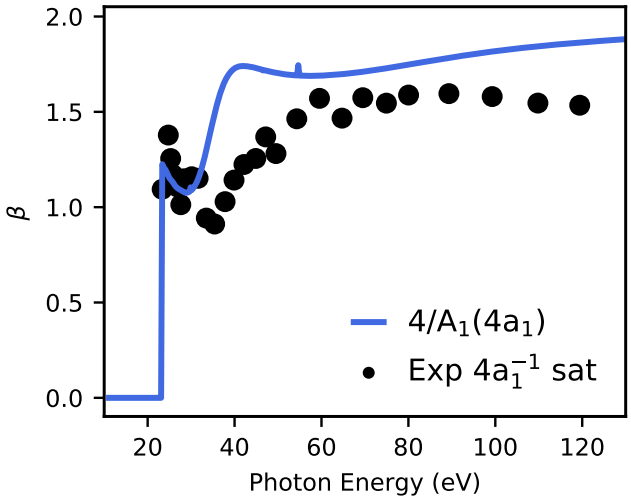


(e) IE = 23.26 eV

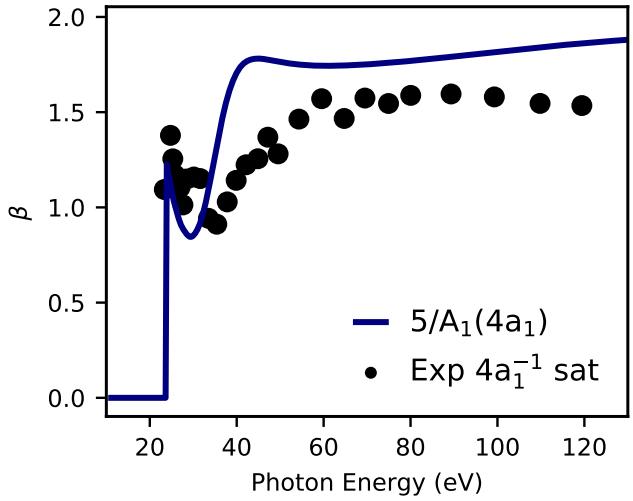


(f) IE = 23.72 eV

Figure S6: $H_2S$: Individual channel asymmetry parameter computed using EOM-CC3/aug-cc-pVTZ Dyson orbital and TD-DFT continuum. Experimental results taken from Ref. [4].

## $CS_2$

Table S9: $CS_2$. Comparison of ionization energies (IE, eV) and spectral strengths ($R_F$. Experimental results are taken from Ref. [5].

| Peak | EOM-CCSD/aVTZ | | EOM-CC3/aVTZ | | EOM-CCSD/aVDZ | | EOM-CC3/aVDZ | | Exp |
|---|---|---|---|---|---|---|---|---|---|
| | IE | $R_F$ | IE | $R_F$ | IE | $R_F$ | IE | $R_F$ | IE |
| X $^2\Pi_g$ | 10.06 | 0.8955 | 9.99 | 0.8556 | 9.90 | 0.8970 | 9.84 | 0.8630 | 10.1 |
| A $^2\Pi_u$ | 13.34 | 0.8315 | 12.84 | 0.7015 | 13.20 | 0.8250 | 12.74 | 0.6993 | 12.9 |
| B $^2\Sigma_u$ | 14.61 | 0.8735 | 14.34 | 0.8189 | 14.45 | 0.8734 | 14.20 | 0.8240 | 14.6 |
| (a) $^2\Pi_u$ | | | 14.82 | 0.0238 | | | 14.74 | 0.0290 | - |
| (b) $^2\Pi_u$ | | | 15.88 | 0.0058 | | | 15.82 | 0.0056 | - |
| C $^2\Sigma_g$ | 16.63 | 0.8179 | 16.09 | 0.6738 | 16.42 | 0.8140 | 15.93 | 0.6798 | 16.2 |
| D $^2\Pi_u$ | 18.24 | 0.0114 | 17.71 | 0.1460 | 17.78 | 0.0136 | 17.60 | 0.1480 | 17.2 |

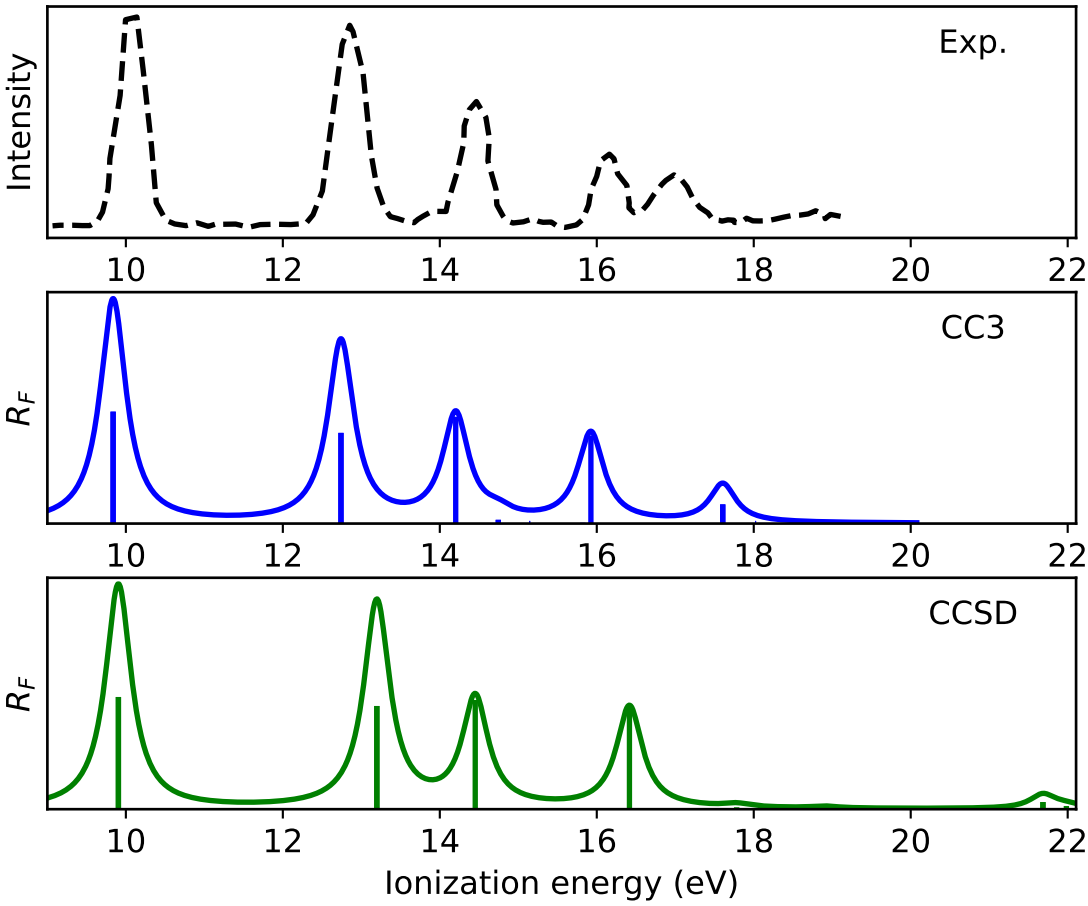


Figure S7: $CS_2$: Photoelelectron spectrum obtained using EOM-CCSD/aug-cc-pVDZ and EOM-CC3/aug-cc-pVDZ. Experimental PES taken from Ref. [5].

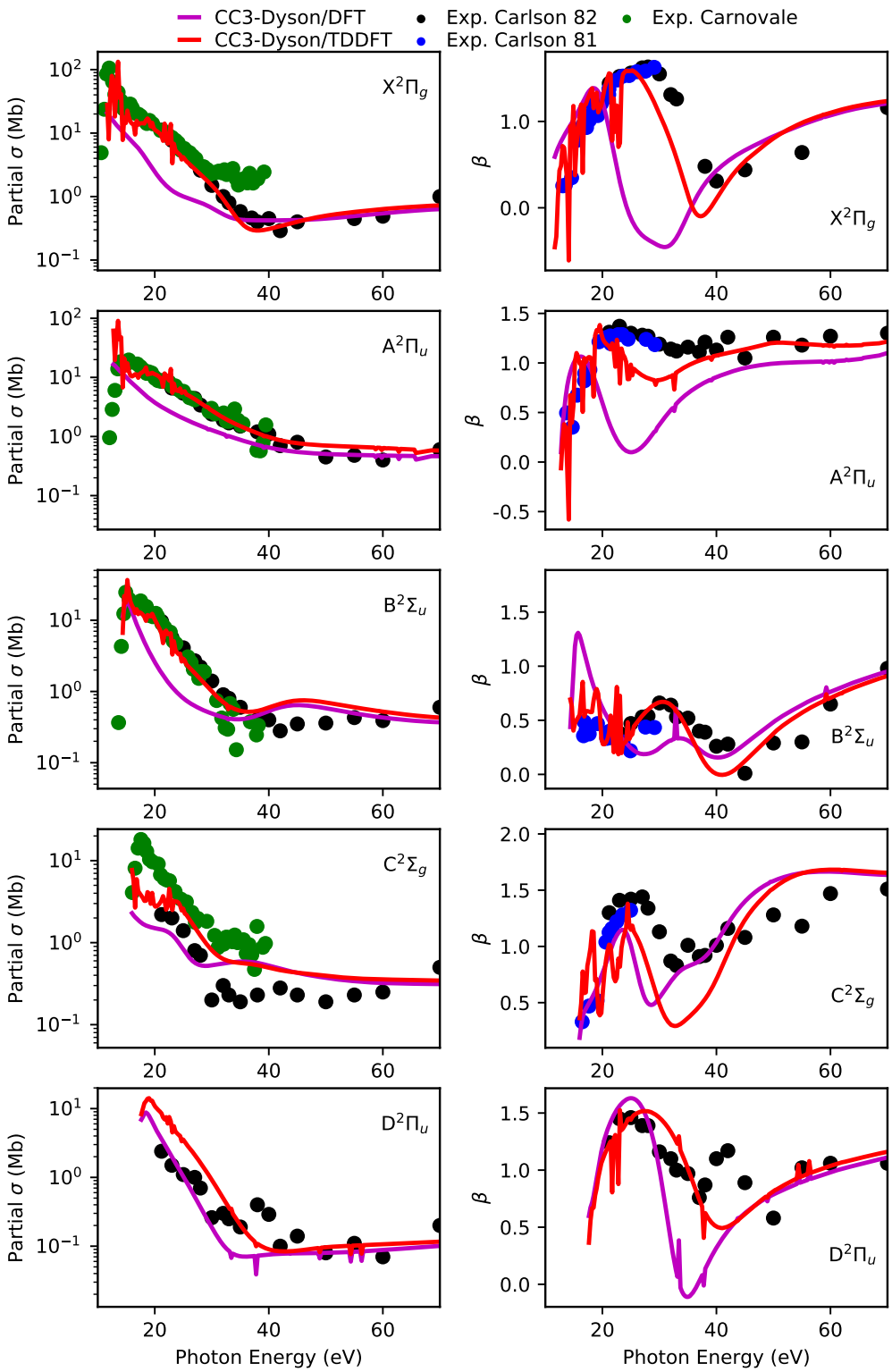


Figure S8: $CS_2$. Partial cross sections and asymmetry parameters of the ionization channels in Table S9. Experimental results (colored dots) are from Ref. [6], [5], [7]. The EOM-CC3/aug-cc-pVTZ Dyson orbitals are used for the bound state description, and DFT and TDDFT for the continuum.

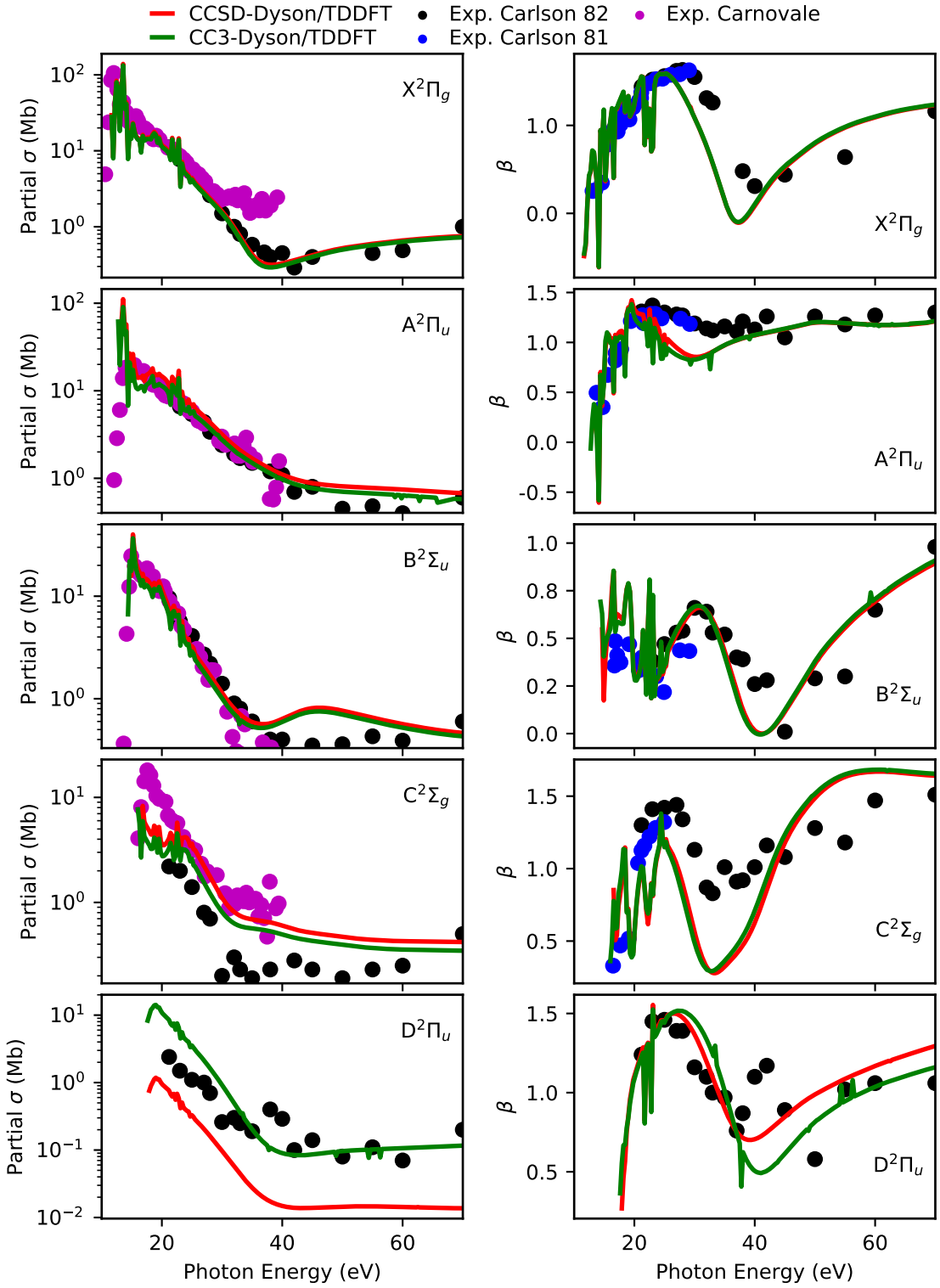


Figure S9: $CS_2$. Partial cross sections and asymmetry parameters, CCSD (red line) versus CC3 (green line) Dyson description of bound state. B-spline TDDFT is used for the continuum part. Experimental results (colored dots) are from Refs. [6, 5, 7]. For the D band, the 17.78 eV and 17.60 eV EOM-CCSD and EOM-CC3 Dyson orbital coefficients were used, respectively.

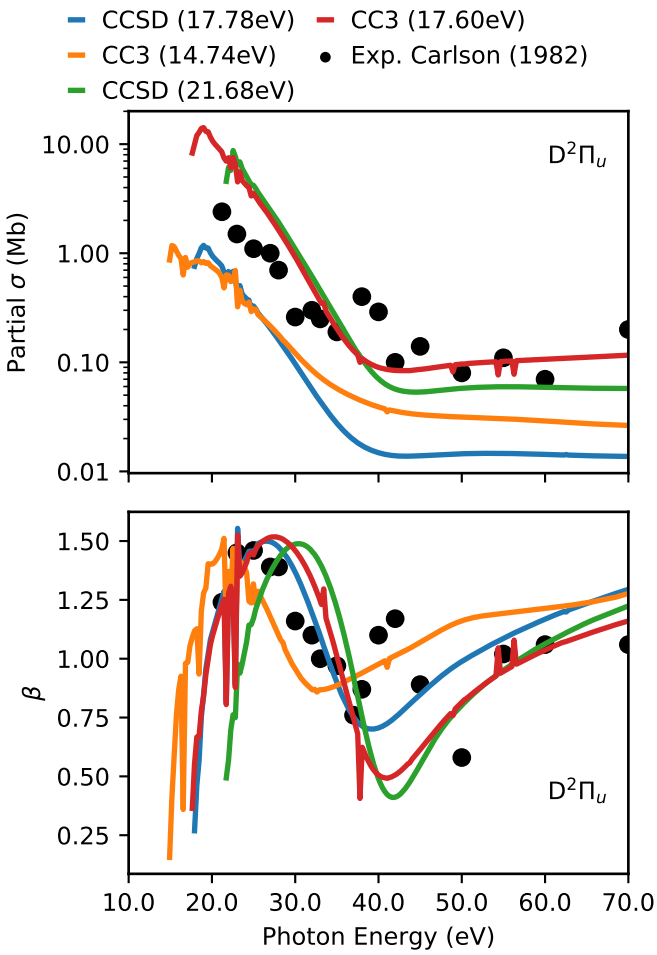


Figure S10: $CS_2$. Partial cross-section and asymmetry parameter for satellite ionization channels. Experimental results are taken from Ref. [5].

## Methyloxirane

Table S10: Methyloxirane: Computed ionization energies and intensities.

| EOM-CCSD/aug-cc-pVTZ | | EOM-CC3/aug-cc-pVTZ | | Exp |
|---|---|---|---|---|
| IE (eV) | $R_F$ | IE (eV) | $R_F$ | IE (eV) |
| 10.37 | 0.8924 | 10.39 | 0.8438 | 10.44 |
| 11.21 | 0.9052 | 11.20 | 0.8743 | 11.32 |
| 13.23 | 0.9070 | 13.18 | 0.8808 | 13.04 |
| 13.43 | 0.9055 | 13.36 | 0.8716 | 13.57 |
| 14.40 | 0.9077 | 14.33 | 0.8764 | 14.46 |
| 15.12 | 0.9067 | 15.03 | 0.8741 | 15.12 |
| 16.13 | 0.8934 | 16.00 | 0.8462 | 16.18 |
| 17.41 | 0.8874 | 17.21 | 0.8266 | 17.22 |
| 20.06 | 0.8686 | | | 19.65 |

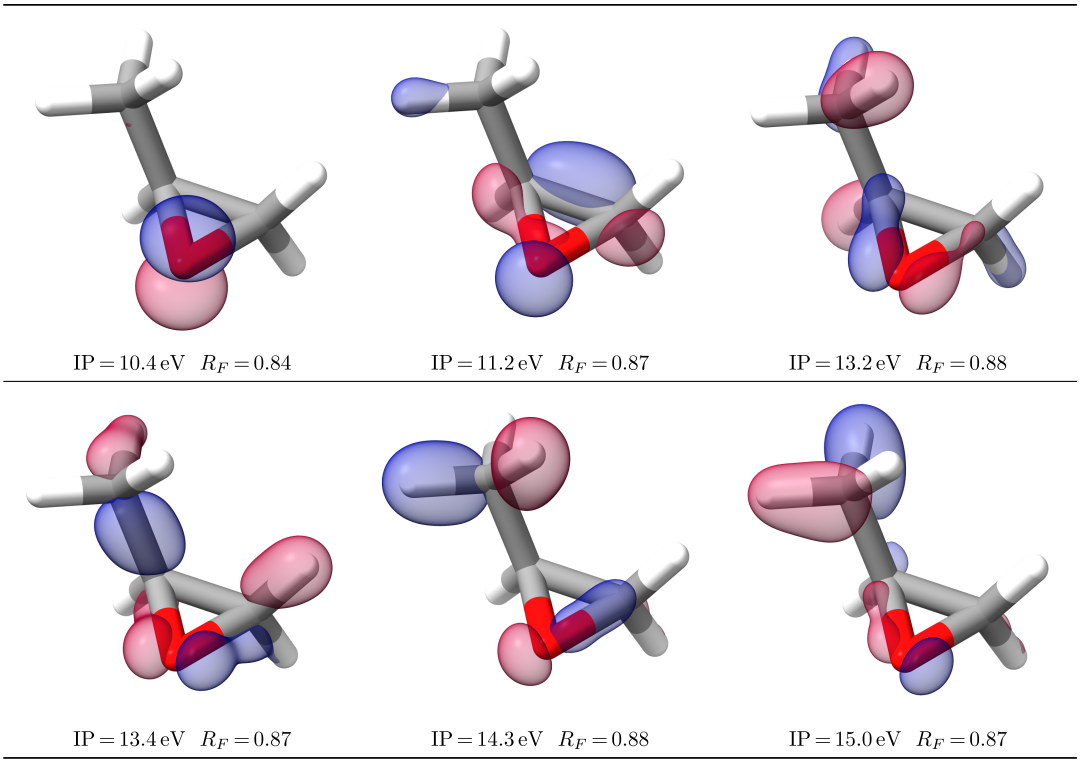


Figure S11: ($S$)-Methyl-oxirane: Right CC3 Dyson orbitals of the six lowest ionized states plotted at an isovalue of 0.1

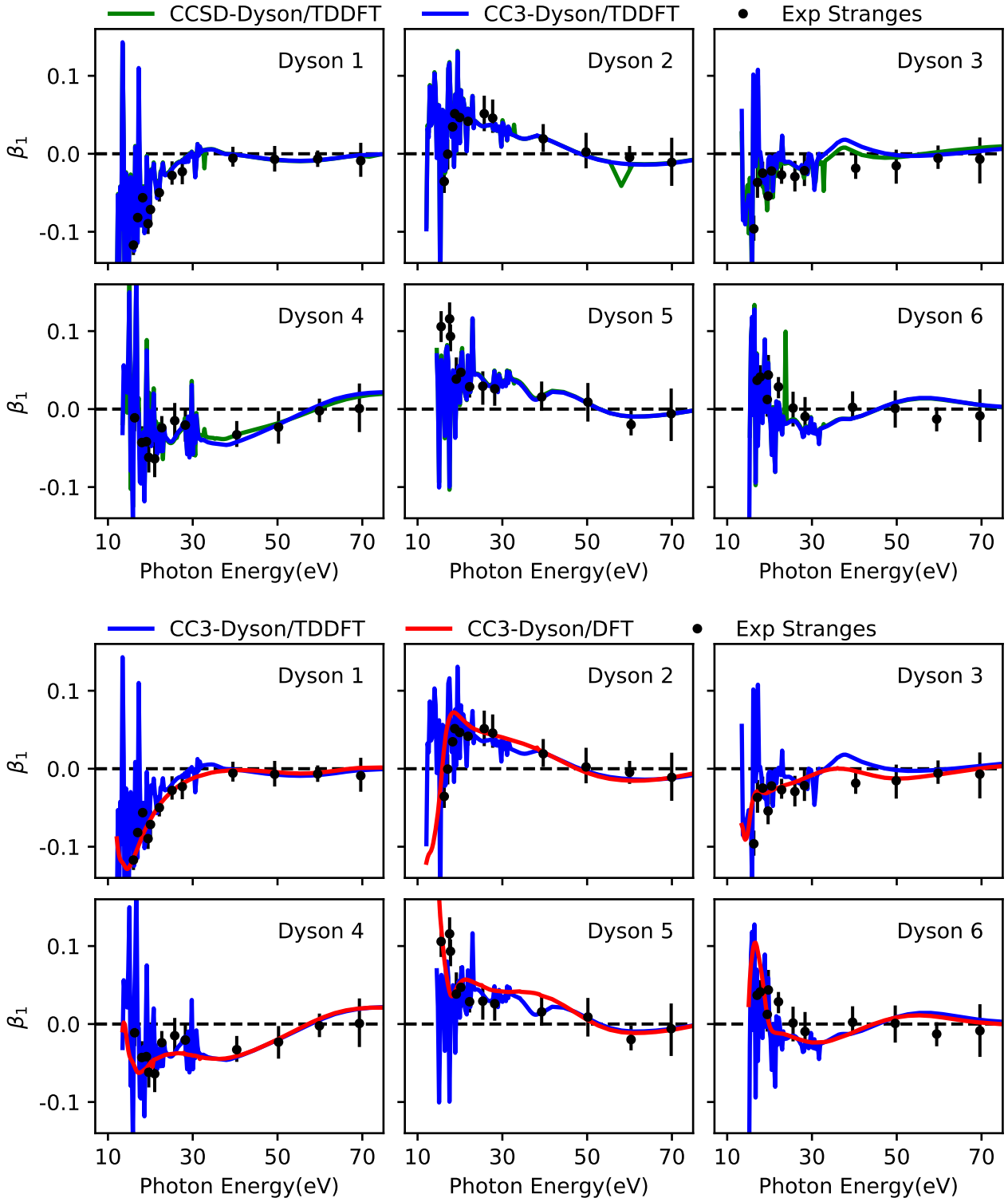


Figure S12: ($S$)-Methyl-oxirane: Photoelectron circular dichroic parameter using CCSD and CC3 Dyson orbitals with TDDFT continuum (first two rows), and CC3 Dyson orbitals with DFT and TDDFT continuum (third and fourth row).

## Geometries

**$H_2O$** (Å)

```
O    0.00000000   0.00000000    0.11730000
H   -0.75720000   0.00000000   -0.46920000
H    0.75720000   0.00000000   -0.46920000
```

**CS** (Å)

```
S   0.00000000   0.00000000    0.41860909
C   0.00000000   0.00000000   -1.11629091
```

**$H_2S$** (Å):

```
S    0.0000   0.0000    0.0000
H   -0.9616   0.0000   -0.9269
H    0.9616   0.0000   -0.9269
```

**$CS_2$** (bohr):

```
C   0.000000   0.0000    0.000000
S   0.000000   0.0000    2.934000
S   0.000000   0.0000   -2.933553
```

**$C_3H_6O$** (bohr)

```
C   -0.28956361    0.08176958    0.92701577
C    1.93885200   -1.15600766   -0.10800484
C   -2.79852375   -0.19094696   -0.27656907
O    1.53613696    1.47730615   -0.46998636
H    1.71860882   -2.32670888   -1.80795335
H    3.52273536   -1.64526642    1.13875511
H   -0.27744501    0.50560530    2.96417187
H   -2.56905279   -0.59002862   -2.30639911
H   -3.89960425    1.56511541   -0.07933409
H   -3.88892566   -1.73605572    0.59599929
```

## References


[1] M. S. Banna, B. H. McQuaide, R. Malutzki, and V. Schmidt. The photoelectron spectrum of water in the 30 to 140 ev photon energy range. *J. Chem. Phys.*, 84(9):4739–4744, 1986.

[2] Neville Jonathan, A. Morris, M. Okuda, K. J. Ross, and D. J. Smith. Photoelectron spectroscopy of transient species. The CS molecule. *Faraday Discuss. Chem. Soc.*, 54:48–55, 1972.

[3] Aurora Ponzi, Celestino Angeli, Renzo Cimiraglia, Sonia Coriani, and Piero Decleva. Dynamical photoionization observables of the CS molecule: The role of electron correlation. *J. Chem. Phys.*, 140(20):204304, 2014.

[4] P. Baltzer, L. Karlsson, M. Lundqvist, B. Wannberg, D. M. P. Holland, and M. A. MacDonald. An experimental study of the valence shell photoelectron spectrum of hydrogen sulphide. *Chem. Phys.*, 195(1):403–422, 1995.

[5] Thomas A. Carlson, Manfred O. Krause, and Frederick A. Grimm. Angle resolved photoelectron spectroscopy of $CS_2$ and COS measured as a function of photon energy from 21 to 70 eV. *J. Chem. Phys.*, 77(4):1701–1709, 1982.

[6] Thomas A. Carlson, Manfred O. Krause, Frederick A. Grimm, John D. Allen, David Mehaffy, Paul R. Keller, and James W. Taylor. Angle-resolved photoelectron spectroscopy of $CS_2$ and COS measured with synchrotron radiation. *J. Chem. Phys.*, 75(7):3288–3292, 1981.

[7] F. Carnovale, M. G. White, and C. E. Brion. Absolute dipole oscillator strengths for photoabsorption and photoionization of carbon disulphide. *J. Elec. Spectr. Rel. Phen.*, 24(1):63–76, 1981.